2

X-692-73-268
PREPRINT

NASA TM X-70467

THE PIONEER XI HIGH-FIELD FLUXGATE MAGNETOMETER

M. H. ACUNA
N. F. NESS

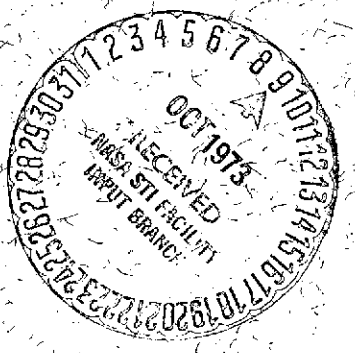

SEPTEMBER 1973

GODDARD SPACE FLIGHT CENTER
GREENBELT, MARYLAND

THE PIONEER XI HIGH-FIELD FLUXGATE MAGNETOMETER

M. H. Acuna

N. F. Ness

August 21, 1973

/

Abstract

This paper describes the High Field Fluxgate Magnetometer Experiment flown aboard the Pioneer 11 spacecraft to investigate Jupiter's magnetic field. The instrument extends the spacecraft's upper limit measurement capability by more than an order of magnitude to 17.3 gauss with minimum power and volume requirements.

Introduction

During the last two decades fluxgate magnetometers have been extensively used in space exploration aboard rockets, satellites and space probes, to study the earth's and interplanetary magnetic field and their interaction with the ambient plasma. Such structures as the sectored Archimedean spiral structure associated with the sun's magnetic field carried out by the solar wind and the earth's magnetospheric cavity and tail are relatively well known today as a result of investigations carried out with these and other instruments.

The Pioneer 10/11 missions to Jupiter provide a unique opportunity to investigate the intense magnetic field which has been predicted for the giant planet, based upon the observed characteristics to its radio emissions in the decimetric and decametric wavelength regions of the spectrum. Typical estimates of the surface equatorial field strength range between 3 and 20 gauss as inferred from the circular polarization of the decimetric radio emissions (Komesaroff et al., 1970). The magnetic field strength obtained from the decametric emission data is about 14 gauss (Carr, 1971) although the exact location of the source is not known. Kemp et al. (1971) have even suggested a field strength of 1000 gauss to account for their observation of a circularly polarized component of the light from Jupiter, but it is unlikely that such a strong field really exists.

Pioneer 10 was launched towards Jupiter on March 2, 1972 and it was followed a year later by Pioneer 11 launched on April 5, 1972. Both spacecraft are spin stabilized and carry a complement of instruments designed to measure the magnetic field, energetic particles and plasma

and in particular, provide detailed knowledge about Jupiter's magnetosphere and radiation belts. Pioneer 10 closes approach to Jupiter occurs Dec. 4, 1973 and Pioneer 11 approximately 1 year later.

The low-field magnetic experiment aboard both spacecraft consists of a vector helium magnetometer capable of measuring fields up to 1.4 gauss. In view of the uncertainties associated with the Jovian magnetic field estimates and to provide additional backup capability to this important experiment, a high-field fluxgate magnetometer described in this paper was added to the Pioneer 11 spacecraft, extending the upper measurement limit to 17.3 gauss.

Instrument Description

The majority of the fluxgate magnetometers used until now were designed to measure weak fields with an upper limit capability of 1-2 gauss imposed by the magnetic geometry used to sense the ambient field. The instrument described here is a single range, triaxial fluxgate magnetometer, designed to measure fields of up to 10 gauss along each orthogonal axis with a maximum resolution of 10^{-2} gauss.

The operating principles are based on the ring-core concept first introduced by Geiger (1961) and further analyzed and developed by Gordon et al. (1965), Acuna and Pellerin (1969), Prindahl (1970), Scouten (1972) and others. One of the distinctive features of the present instrument is that it does not operate on the second harmonic principle in a strict sense, but rather it derives its output signal from the short pulses induced in the pick-up winding of the sensor when an external magnetic field is applied. In addition, the ring-core geometry is ideally suited to multiple-axis sensing applications when the orientation of the sensing axes are parallel to the plane of the core. We thus can obtain response along two orthogonal axes with a single ring core. These features plus minimum power consumption, allow the realization of an instrument of extreme simplicity and reliability.

A block diagram of the Pioneer-11 instrument is shown in figure 1. The major functional blocks are: a) Sensors, b) Analog-to-digital converters and output buffer, c) Timing logic and d) Power switching and interface circuits. Since the overall power consumption is only 300mw, the instrument derives its power from the Goddard Cosmic Ray Telescope Experiment aboard the spacecraft through a set of current limited transistor switches. The

instrument is mounted on the spacecraft experiment platform as shown in figure 2, in the immediate vicinity of the CRT package. The spacecraft magnetic field at this location is much smaller than the quantization error of the A/D converters and has no influence upon the performance of the instrument. A photograph of the complete magnetometer without its case is shown in figure 3. Total weight and volume are 272 gms and 546 cm^3 respectively.

a) Sensors

The sensors consist of two orthogonally mounted ring cores which are driven cyclically to saturation by their associated oscillators at a frequency of 8 KHZ. Two orthogonal sense windings diametrically wound around each core, provide sensitivity along three orthogonal axes plus a redundant measurement along one of the axes. A schematic representation of the construction of each sensor is shown in figure 4. This type of sensor design has been extensively used in aspect magnetometers flown aboard sounding rockets (Acuna and Pellerin, 1969). The high field measurement capability of the present sensors is obtained by maximizing the external field attenuation factor (Bozorth, 1942, 1951) given by,

$$A = \frac{H}{He} = 1 + \mu\,(L/d)^{-\alpha} \qquad (1)$$

where H is the applied excitation, He the effective excitation seen by the sensor and μ the permeability of the magnetic material. The parameter α is determined by the permeability and for $\mu = \infty$ it takes the value $\alpha = 1.72$ The quantity L/d for the case of a ring core may be approximated as the ratio between the core diameter L and the diameter d of a rod of equivalent cross-sectional area to that of the magnetic core. A core

satisfying the high attenuation criteria (small L/d, high μ) was selected from commercially available 4-79 Mo-Permalloy tape wound units with L/d = 4.

The effective permeability μ to be used in (1) is a function of the external excitation applied to the sensor and non-linear behavior is to be expected for large values of H. Since the instrument is a single range magnetometer, this characteristic was used to increase the dynamic range over which measurements can be made with a given A/D converter quantization step size while maintaining acceptable relative accuracy. The overall response thus approaches a logarithmic function of the excitation field.

The cores perform the dual function of magnetic field sensors and frequency control devices for their drive oscillators. A schematic diagram of the sensor-oscillator circuit is shown in figure 5. The drive oscillator is a standard square wave inverter circuit to which current feedback has been added to obtain constant peak drive as a function of temperature. When the voltage drop across resistors R_1 or R_2 reaches the turn-on base emitter voltage of Q_1 or Q_2, the circuit will switch states due to the decreasing base drive which is supplied to the inverter transistors. Thus, the switching points are not controlled by the inverter transistors gain but by the desired peak current flowing in the drive winding of the core. The voltage developed across capacitor C_1 by the base currents of Q_3 and Q_4 provides additional drive stabilization. When the core reaches saturation, capacitor C_6 discharges across the drive winding; this current adds to that provided by the inverter transistors driving the core deeper into saturation.

The signals from the pick-up windings are applied to two phase

sensitive detectors. The reference signal for these detectors is generated by differentiation and full-wave rectification of the square wave drive to obtain a series of unidirectional pulses. Figures 6 shows the output waveform obtained across the pick-up windings when an external field excitation is applied to the sensors, and its time relationship with respect to the reference signal. The value of the damping resistors (R_{11}) across the pick-up windings is chosen such as to critically damp or overdamp the resonant circuit formed with the stray and distributed capacitances. No tuning of the sense winding to the second harmonic of the drive frequency is required to ensure proper operation of the sensor and phase sensitive detector circuits. Figure 7 shows a typical response curve obtained with the sensors described above. At 8 KHZ power consumption is less than 60 mw for each two-axis sensor.

b) Analog-to-digital converters and Output Buffer

The d.c. output signals from the sensors corresponding to 3 othogonal axes are filtered (0-1 HZ) and digitized by three 10-bit single ramp A/D converters of the Wilkinson type. A block diagram of this subsystem is shown in figure 8. The X, Y, and Z signals are sampled and digitized simultaneously upon the occurrence of a "Roll Index Pulse". This pulse is generated by the spacecraft and is related to the time of crossing of a reference line through the ecliptic plane. The RIP pulse fires a one-shot for the duration of the A/D conversion period to provide a "busy" gate and transfer the digital information into temporary storage. The counters for the A/D converters are custom PMOS devices providing two levels of storage. The trailing edge of the busy gate transfers the counter contents into temporary storage and resets it to zero. The 36-bit PMOS output

buffer is loaded in 4-bit bytes upon the occurrence of a "Load" pulse. Its contents are then shifted out in 6 bit blocks into the spacecraft Digital Telemetry Unit as explained below.

c) Timing Logic

The timing logic provides the necessary control signals for the operation of the instrument and generates a synchronizing gate for proper decoding of the digital information supplied to the DTU.

The fluxgate magnetometer data is multiplexed into one of the science subcom formats available in the spacecraft. Two 'Word Gates' per subcom cycle are assigned to the instrument, each gate corresponding to six bits of data being shifted into the DTU. Thus, 3 subcom cycles are required to read out the contents of the output buffer. At 2,048 BPS a complete subcom cycle requires 6 seconds and a complete (3 axis) measurement is obtained every 18 seconds depending upon the roll rate of the spacecraft. (nominal: 1 rev/12 sec.).

A timing diagram is shown in figure 9. The output buffer is loaded by the first "Science Subframe Rate Pulse" occurring after a "Roll Index Pulse" has been accepted by the system. Once the system accepts a Roll Index Pulse it locks-out this input until the output buffer contents have been read out by the spacecraft. The synchronization gate is generated during the interval between the first and second Science Subframe Rate Pulses and is used to saturate a buffer amplifier associated with the redundant axis data which is fed to the DTU in analog form. This signal is digitized by the DTU with 6-bit resolution.

d) Power Switching Circuits

It has been mentioned that the fluxgate magnetometer derives its

power from the Cosmic Ray Telescope Experiment aboard the spacecraft. Since several voltages are used and the sensors form an integral part of the package, magnetic latching relays can not be used to provide power switching functions. In addition, relay switches do not allow for the implementation of current limiting capabilities into the switching function without incurring unacceptable voltage drops in the circuits. An acceptable compromise is to use saturated transistor switches for this purpose. Figure 10 shows two basic circuits used in the experiment to switch positive or negative voltages, controlled by a common flip-flop. A 'Calibrate' pulse derived from the CRT experiment is used to toggle this flip-flop and accomplish the desired power control functions.

General

The complete instrument, including sensors, is housed in a 10.8 x 7 x 4.5 cm box. As shown in figure 3, the sensors are arranged as to minimize the influence of permeable materials present in integrated circuit packages, transformer cores, etc. Typical hysteresis observed after exposure to 25 gauss fields in less than 1 part in 10^3 (one count). Temperature stability is $\pm$0.25% from -20 to +40 degrees centigrades in spite of the fact than no d.c. feedback is used in the sensors as is customary in fluxgate magnetometers. A large fraction of this drift is attributable to the single ramp A/D converter, but minimal power consumption requirements precluded the use of more stable converters.

Acknowledgments

The authors wish to express their appreciation of the outstanding support provided by Mr. D. Stilwell of the CRT experiment group, Messrs. C. Bayne, R. Cummings and R. Markley of the Microelectronics and

Packaging Branch, Mr. H. White of the Data Techniques Branch, the Space and Tactical Systems Corporation, Bedford, Mass. and the Pioneer Project Office. This support made possible the construction, test and successful integration of a fully spaceflight qualified instrument in the very short period of 3 months.

References

Acuna, M. H. and Pellerin, C. J., 1969, IEEE Trans. Geo. Elect., GE-7, 252-260.

Bozorth, R. M. and Chapin, D. M., 1942, J. Appl. Phys., 13, 320-326.

Bozorth, R. M., 1951, "Ferromagnetism", D. Van Nostrand, Co., Princeton, N. J.

Carr, T. D., 1971, Proceedings of the Jupiter Radiation Belt Workshop, NASA-JPL, TM 33-543.

Geiger, W. A., 1965, AIEE Trams., 81, 65-73.

Gordon, D. L., Lundsten, R. H. and Chiarodo, R. A., 1965, IEEE Trans. Magnetics, MAG-1, 330-337.

Kemp, J. D., Swedlund, J. B., Murphy, R. E. and Wolstencroft, R. D., 1971, Nature, 231, 169-170.

Komesaroff, M. M., Morris, D. and Roberts, J. A., 1970, Ap. Letters, 7, 31-36.

Primdahl, H., 1970, IEEE Trans. Magnetics, MAG-6, 376-383.

Scouten, D. D., 1972, IEEE Trans. Magnetics, MAG-8, 223-231.

Figure Captions

Figure 1	Block diagram of the Pioneer 11 fluxgate magnetometer
Figure 2	The Pioneer 11 spacecraft and the location of major scientific experiments.
Figure 3	The complete Pioneer 11 instrument.
Figure 4	Schematic representation of the sensors. Two orthogonal sense windings are shown.
Figure 5	Simplified diagram of the sensor electronics.
Figure 6	Output and reference waveforms obtained with the high field sensor.
Figure 7	D.C. output voltage vs. applied field for a typical sensor.
Figure 8	Analog-to-digital converters and output buffer block diagram.
Figure 9	Timing Waveforms for the Experiment
Figure 10	Power switching circuits.

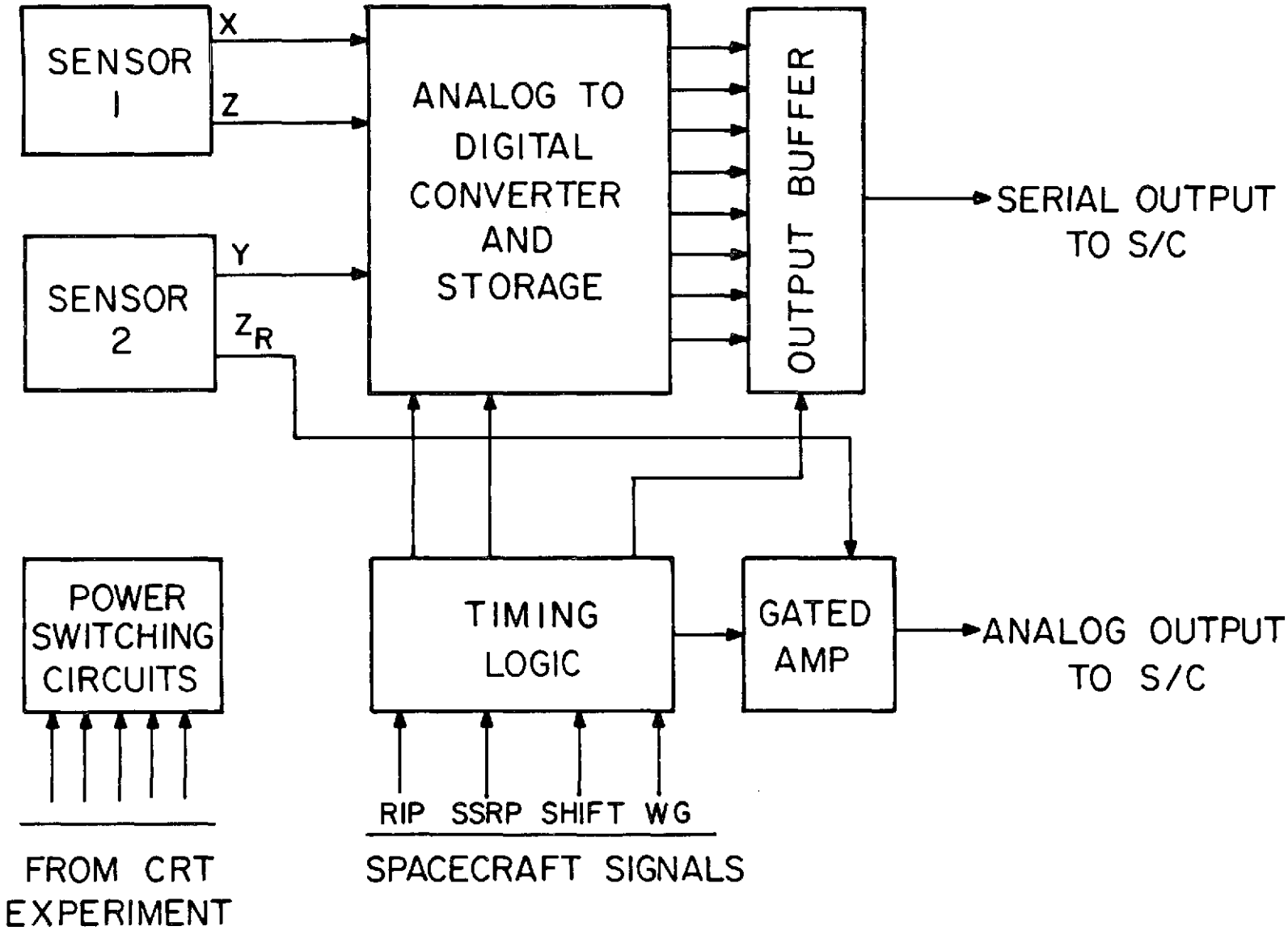
SENSOR 1
X
Z
SENSOR 2
Y
Z_R
ANALOG TO DIGITAL CONVERTER AND STORAGE
OUTPUT BUFFER
SERIAL OUTPUT TO S/C
POWER SWITCHING CIRCUITS
TIMING LOGIC
GATED AMP
ANALOG OUTPUT TO S/C
RIP
SSRP
SHIFT
WG
FROM CRT EXPERIMENT
SPACECRAFT SIGNALS

Fig. 1

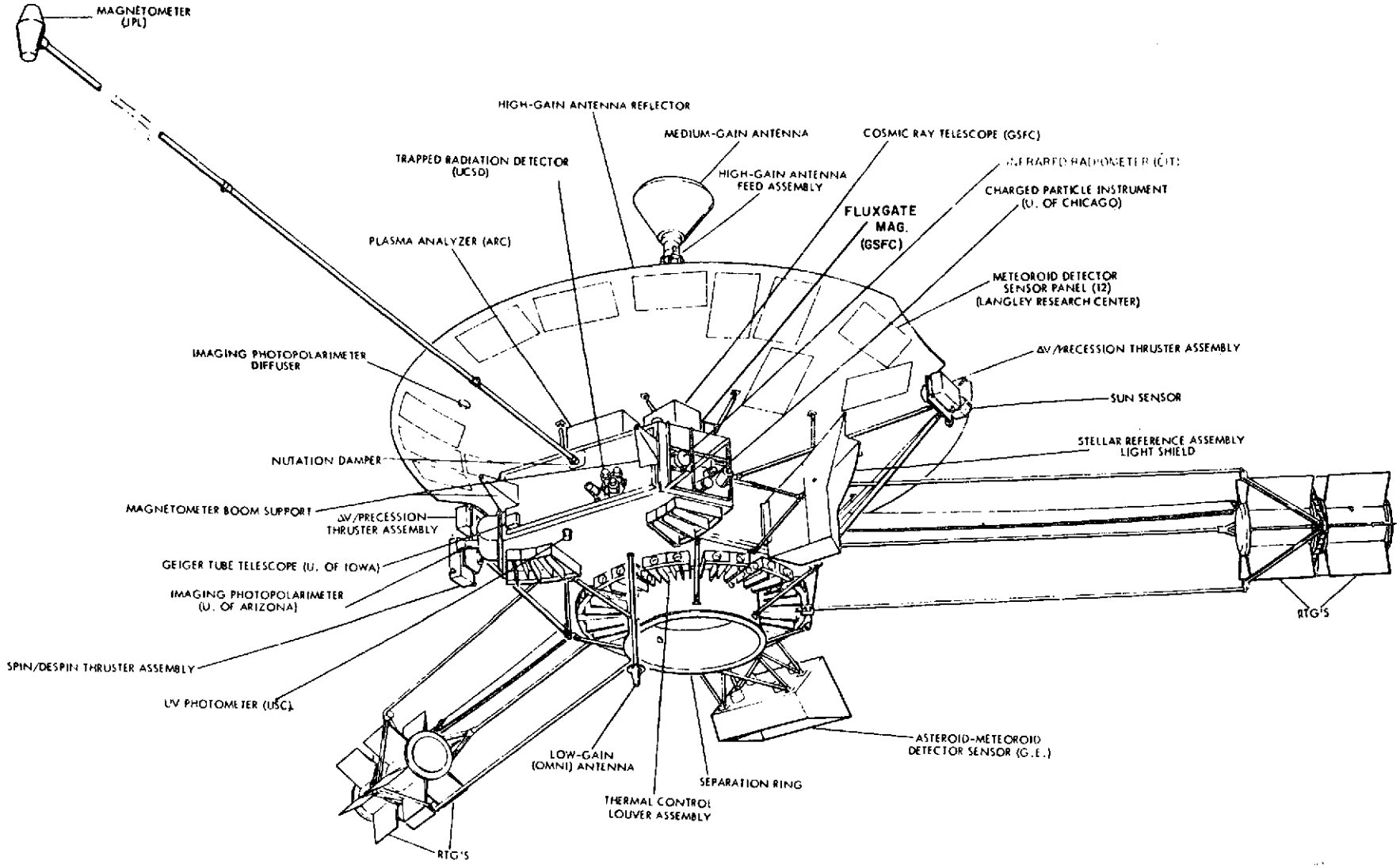
MAGNETOMETER (JPL)
HIGH-GAIN ANTENNA REFLECTOR
MEDIUM-GAIN ANTENNA
COSMIC RAY TELESCOPE (GSFC)
TRAPPED RADIATION DETECTOR (UCSD)
HIGH-GAIN ANTENNA FEED ASSEMBLY
CHARGED PARTICLE INSTRUMENT (U. OF CHICAGO)
FLUXGATE MAG. (GSFC)
PLASMA ANALYZER (ARC)
METEOROID DETECTOR SENSOR PANEL (12) (LANGLEY RESEARCH CENTER)
IMAGING PHOTOPOLARIMETER DIFFUSER
ΔV/PRECESSION THRUSTER ASSEMBLY
SUN SENSOR
STELLAR REFERENCE ASSEMBLY LIGHT SHIELD
NUTATION DAMPER
MAGNETOMETER BOOM SUPPORT
ΔV/PRECESSION THRUSTER ASSEMBLY
GEIGER TUBE TELESCOPE (U. OF IOWA)
IMAGING PHOTOPOLARIMETER (U. OF ARIZONA)
RTG'S
SPIN/DESPIN THRUSTER ASSEMBLY
UV PHOTOMETER (USC)
ASTEROID-METEOROID DETECTOR SENSOR (G.E.)
LOW-GAIN (OMNI) ANTENNA
SEPARATION RING
THERMAL CONTROL LOUVER ASSEMBLY
RTG'S

74

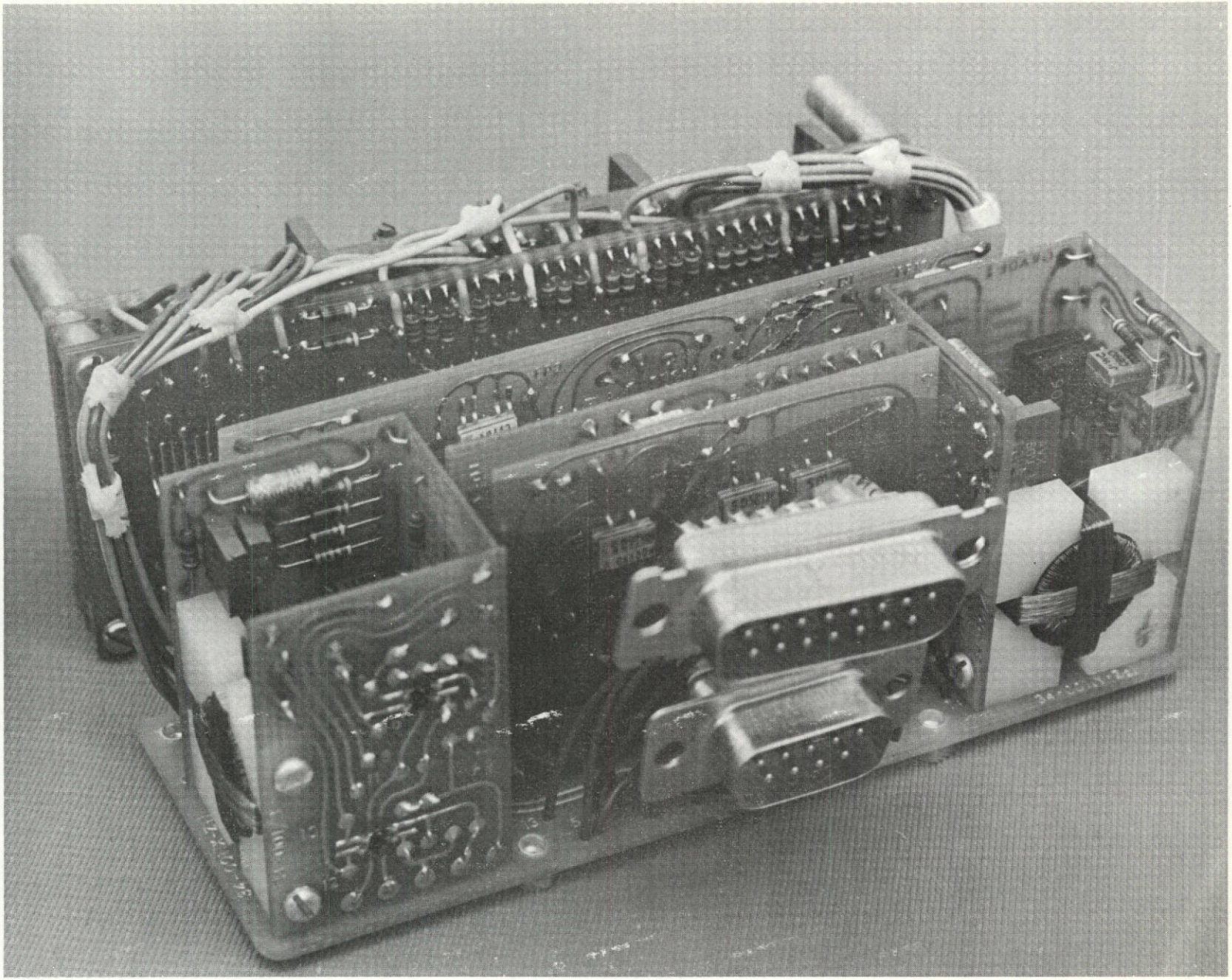

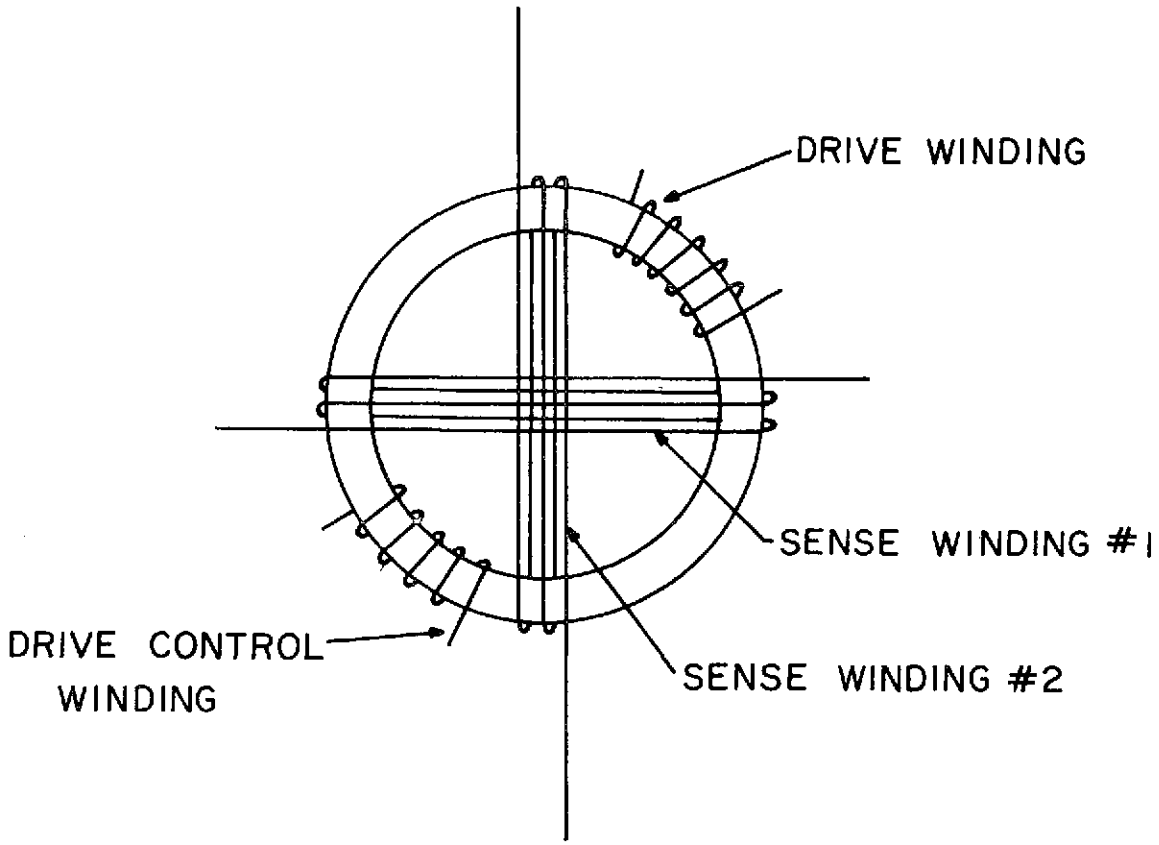
DRIVE WINDING
SENSE WINDING #1
SENSE WINDING #2
DRIVE CONTROL WINDING

Fig. 4

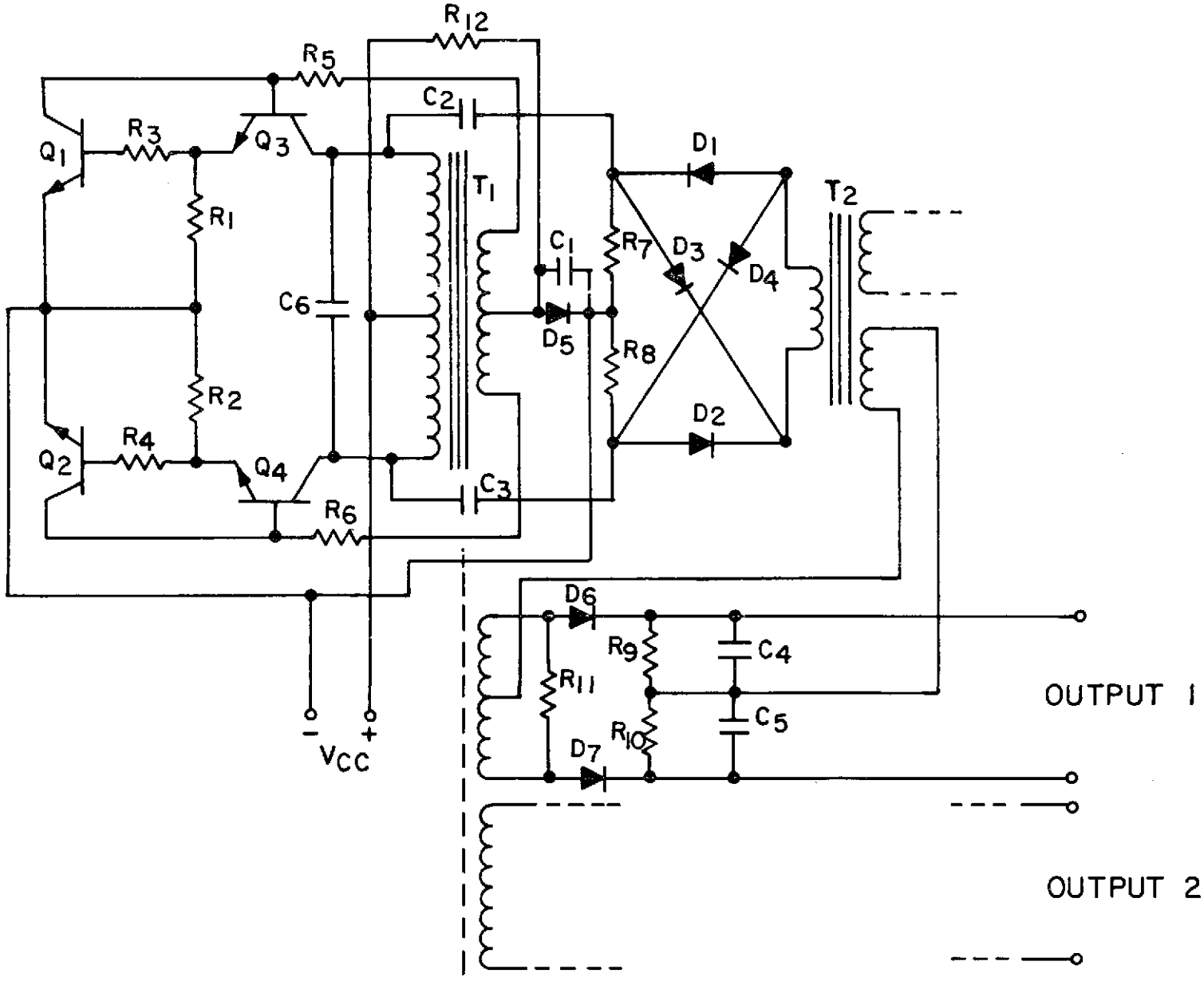
R12
R5
C2
R3
Q1
Q3
T1
D1
T2
R1
C1
R7
D3
D4
C6
D5
R8
R2
D2
R4
Q2
Q4
C3
R6
D6
R9
C4
R11
OUTPUT 1
C5
R10
D7
VCC
OUTPUT 2

Fig. 5

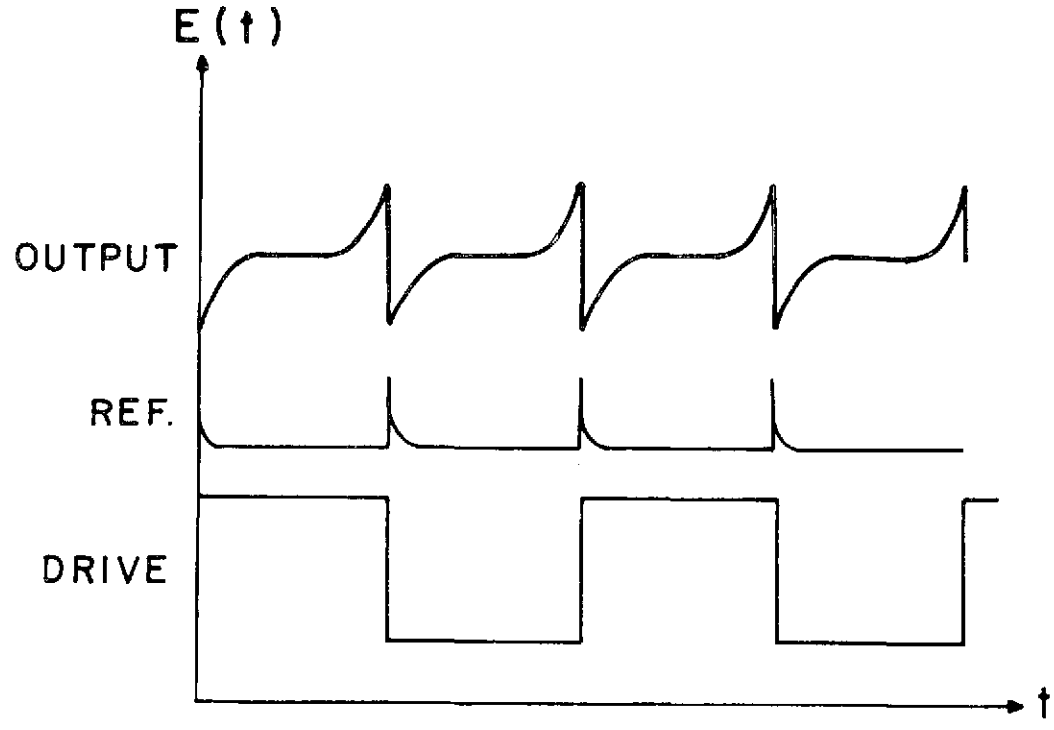

Fig. 6

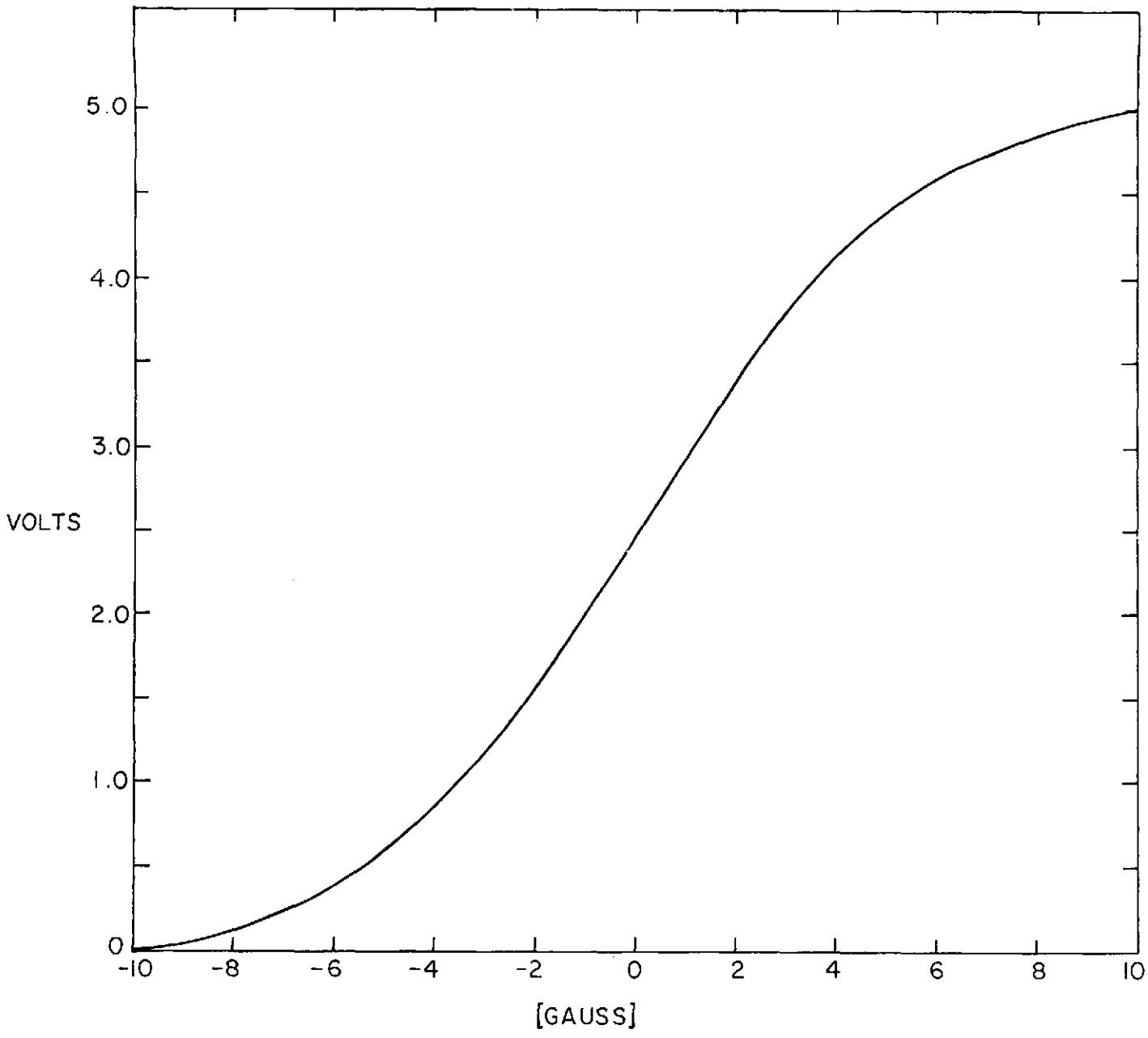

Fig. 7

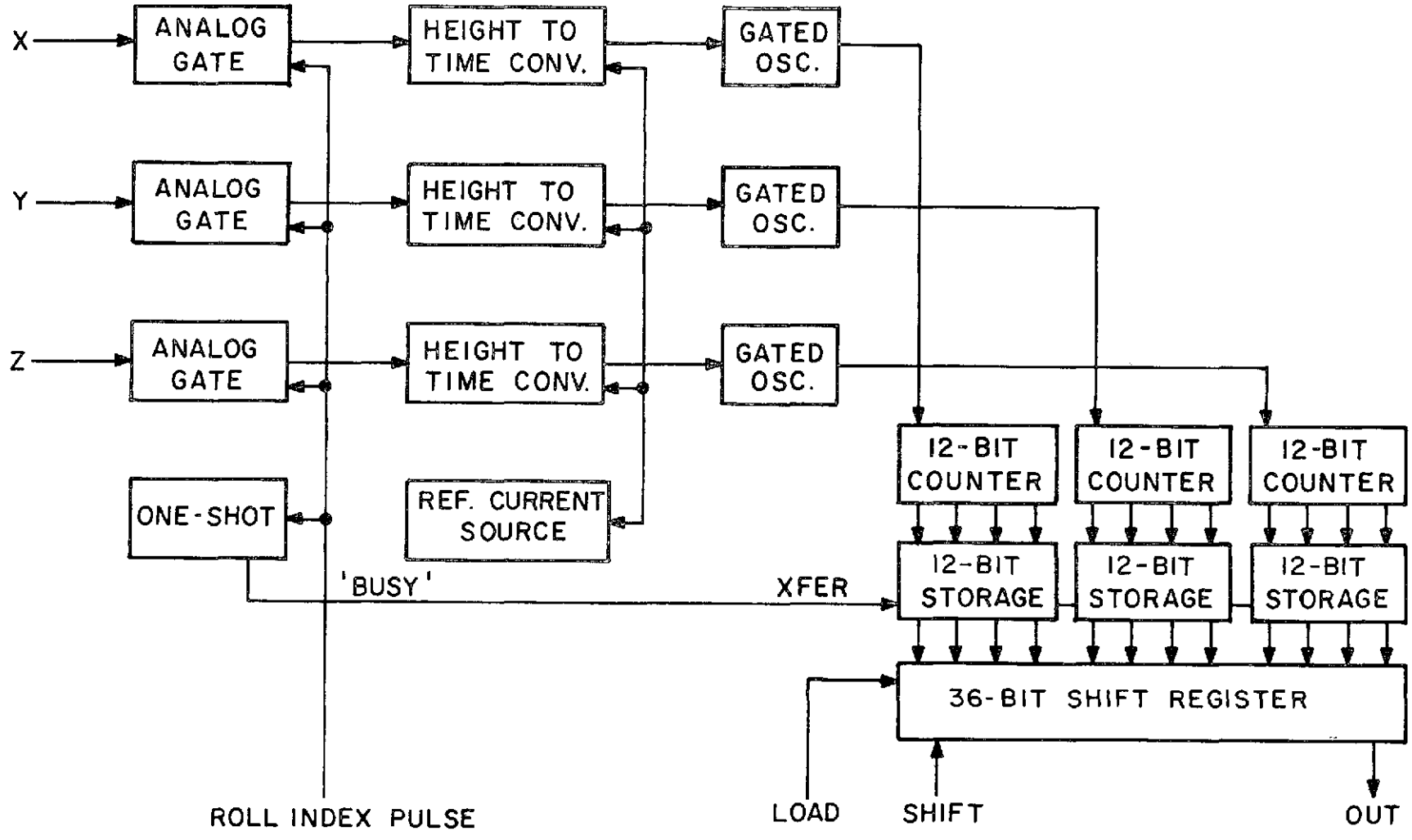
X
Y
Z
ANALOG GATE
ANALOG GATE
ANALOG GATE
HEIGHT TO TIME CONV.
HEIGHT TO TIME CONV.
HEIGHT TO TIME CONV.
GATED OSC.
GATED OSC.
GATED OSC.
ONE-SHOT
REF. CURRENT SOURCE
'BUSY'
XFER
12-BIT COUNTER
12-BIT COUNTER
12-BIT COUNTER
12-BIT STORAGE
12-BIT STORAGE
12-BIT STORAGE
36-BIT SHIFT REGISTER
ROLL INDEX PULSE
LOAD
SHIFT
OUT

Fig. 8

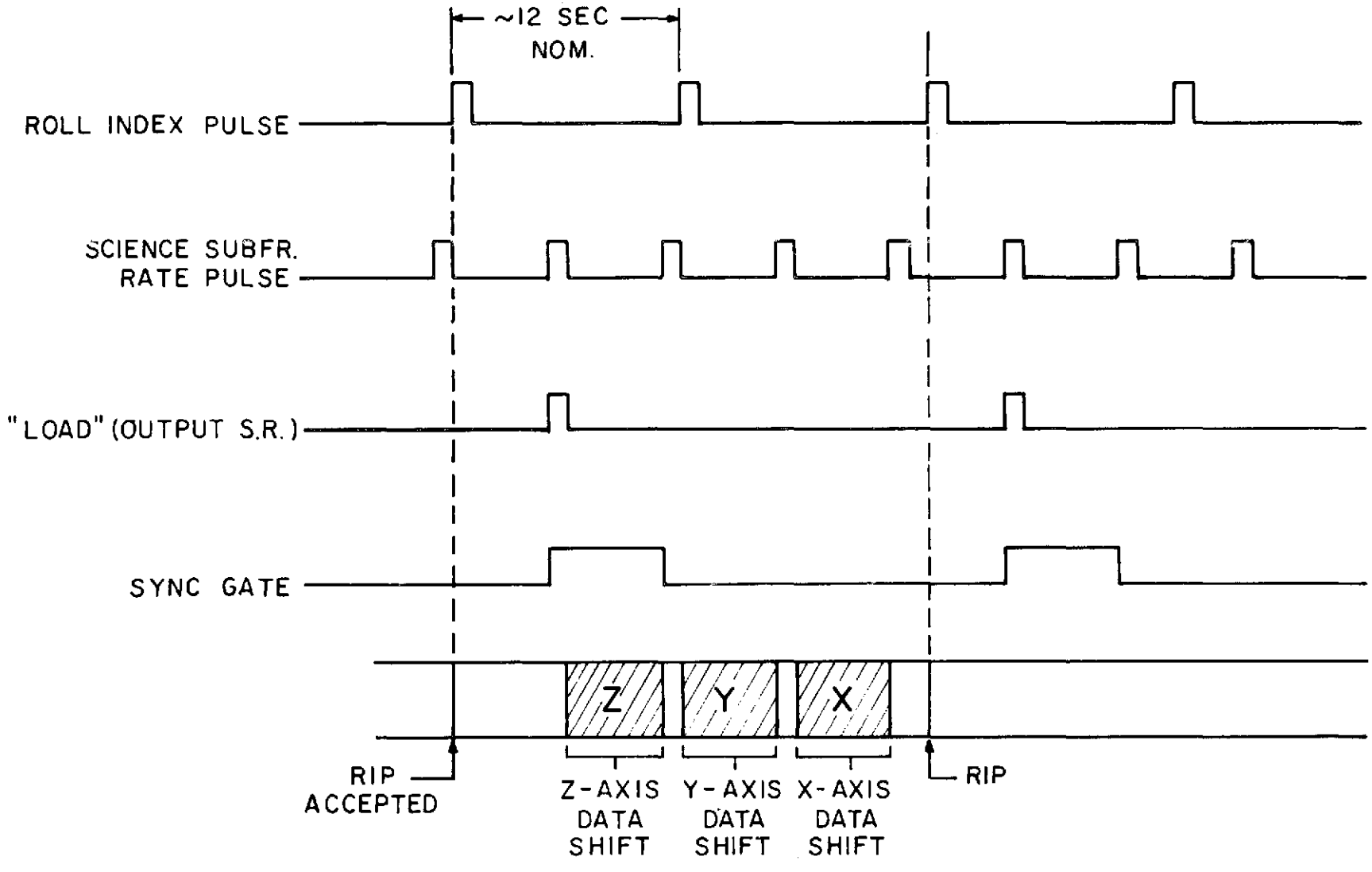
~12 SEC
NOM.
ROLL INDEX PULSE
SCIENCE SUBFR.
RATE PULSE
"LOAD" (OUTPUT S.R.)
SYNC GATE
Z
Y
X
RIP
ACCEPTED
Z-AXIS
DATA
SHIFT
Y-AXIS
DATA
SHIFT
X-AXIS
DATA
SHIFT
RIP

Fig. 9

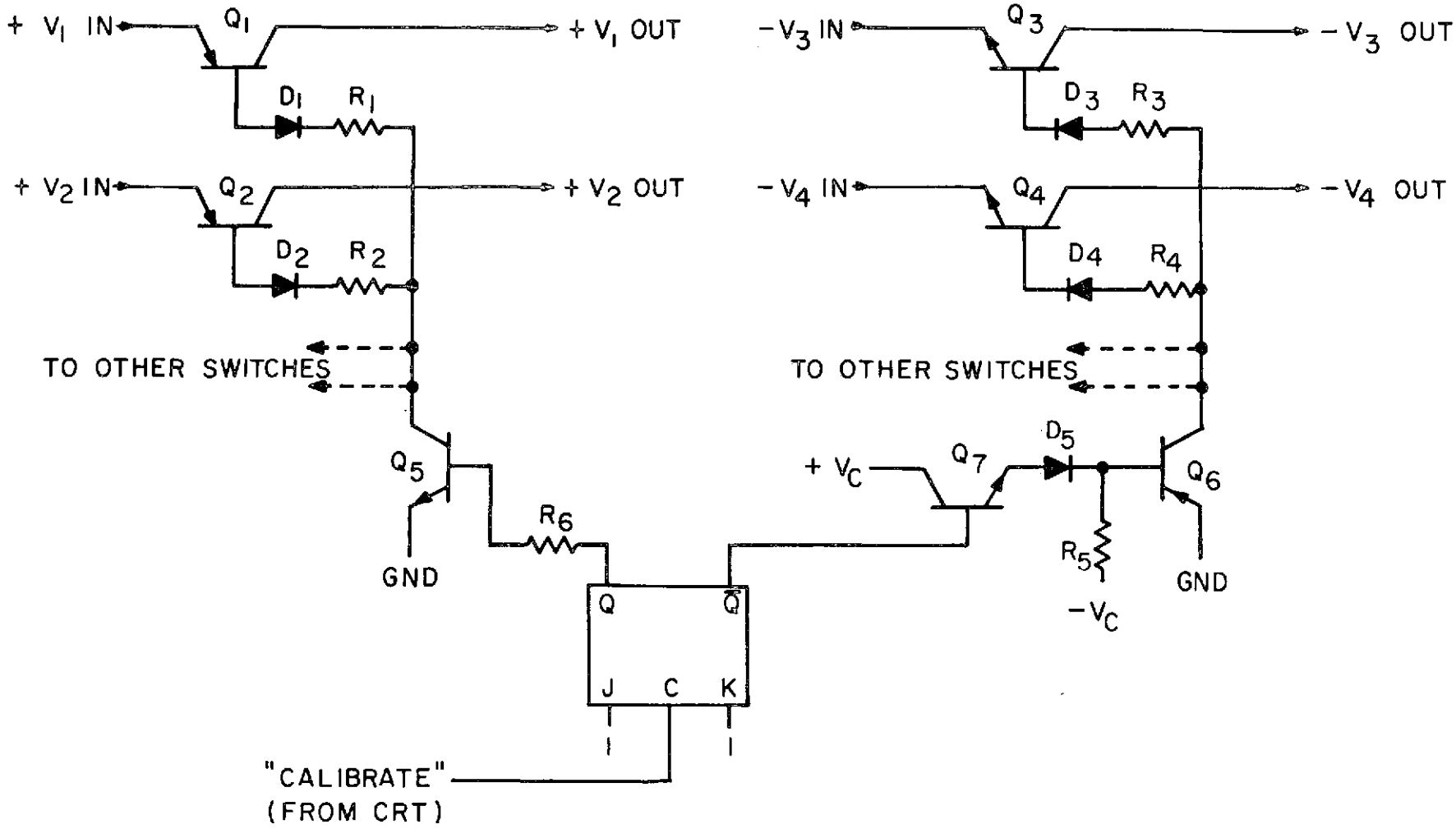

Fig. 10

NASA–GSFC